3.1 Bericht Teilprojekt 1

3.1.1 Titel / Title

Molekulardynamik-Simulation von Struktur, Bildung und Reaktivität von Molekülen und Clustern

Molecular dynamics simulation of structure, formation and reactivity of molecules and clusters

3.1.2 Berichtszeitraum / reported period

01.08.2003 - 31.07.2006

3.1.3 Projektleiter / principle investigator

Seifert, Gotthard, Prof. Dr., Dipl.-Chem. Universitätsprofessor,
Institut für Physikalische Chemie, Technische Universität Dresden

Scholz, Reinhard, Dr., Dipl.-Phys., Oberassistent,
Technische Universität Chemnitz (bis Dezember 2006)
Technische Universität München (seit März 2006)

3.2 Zusammenfassung / Abstract

3.2.1 Wortlaut des Antrags / abstract of the proposal

Das vorliegende Projekt soll zum Verständnis der Elementarschritte beitragen, welche die dynamische Evolution der interstellaren Materie kontrollieren. Dazu werden Verfahren der Dichte-Funktional Theorie (DFT) und die Dichte-Funktional basierte „tight-binding“ Methode angewendet, die eine hohe Genauigkeit und eine herausragende numerische Leistungsfähigkeit kombinieren. Die Reaktionen der Moleküle und Cluster werden mit statischen Rechnungen des optimalen Reaktionsweges und durch dynamische Simulationen der Kollisionen zwischen Molekülen, Clustern und den entsprechenden Ionen untersucht. Insbesondere soll die Bildung kleiner Kohlenwasserstoffspezies durch Simulation der Stöße zwischen Kohlenstoffclustern und Clusterionen mit CH_x und mit H_2 untersucht werden. Weiterhin soll die Bildung von zyklischen Kohlenwasserstoffen als Elementarschritt für die Bildung von PAH’s aufgeklärt werden.

The present project shall contribute to an understanding of the elementary steps controlling the dynamical evolution of interstellar matter. The methods applied will be the density-functional theory (DFT) and the density-functional based tight-binding (DFTB) method, combining a high precision with an outstanding numerical performance. The reactions of molecules and clusters will be investigated by static calculations of the optimum reaction path and by dynamical simulations of the collisions between molecules, clusters, and the corresponding ions. Especially the formation of small hydrocarbon species by simulations of collisions between carbon clusters and cluster ions with CH_x and with H_2 will be studied. Furthermore, the formation of cyclic hydrocarbons as elementary steps for the formation of polycylic aromatic hydrocarbons (PAH) shall be clarified.

3.2.2 Zusammenfassung des Berichts / abstract of the report

In the course of the present project, we have studied formation processes of carbon clusters and hydrocarbons restricted to ultra-low temperatures and densities. The method used for these studies is the density functional theory (DFT).

Our approach is based on quantum molecular dynamic simulations of the collisions between molecular reactants within a statistical framework. In particular, the simulations were conducted by a modification of the DFT, the density-functional based tight binding (DFTB) method, which combines a high precision with an outstanding numerical performance.

On the other hand, the characteristics of single reaction channels were studied by the nudged elastic band method (NEB). The properties of the reactants and the products, as well as the intermediates and the transition states of the reaction channels were refined by modest levels of quantum chemistry.

The investigations comprised ion-molecule reactions of mono-, di-, tri- and tetravalent small interstellar hydrocarbon molecules with carbon clusters and hydrocarbons (CH, HCCC, H_2CC, H_2CCC, H_2CCCC, C_2 + $C_xH_y^+$ and $HCCCH_2^+$ + C_xH_y, with x=5-24 and y=0-12). Special emphasis was put in the study of the formation channels of aromatic structures .

Additionally, for a small reference system (C_3), the excited states were analysed with time-dependent density functional theory. The suitability of different excited electronic configurations for the reaction $C_3 + C_3 \rightarrow C_6$ was investigated for selected highly symmetric relative orientations of the reactants.

3.3 Ausgangsfragen, neuster Stand der Forschung / Initial goals, current status of the field

The project was established to contribute to an understanding of the elementary steps which control the dynamical evolution of interstellar matter. The focus was set on the polycyclic hydrocarbon, especially polycyclic aromatic hydrocarbon (PAH), growth mechanisms.

These molecules are known to be part of the interstellar and circumstellar matter. Evidences of their presence comes the infrared (IR) emission bands of different astronomical objects [*Leger1984, Allamandola1985*]. Moreover, interstellar PAHs are considered to be an intermediate stage between the gas and the dust phases of interstellar matter [*Duley1981, Leger1989*]. They are expected to exist in a complex statistical equilibrium of different charge and hydrogenation states. In addition, due to IR fluorescence and photoelectric heating processes, PAH account for a substantial fraction of the total interstellar carbon budget and contribute to the energy balance of the galaxy [*Bakes1994, Habart2001*].

Different formation mechanisms can be responsible for the abundance of polycyclic hydrocarbons and PAHs: a) circumstellar chemistry [*Allamandola1989*], b) shattering of carbonaceous dust grains [*Jones1996*], c) photo-induced destruction of carbonaceous cluster [*Brechignac2005*], and d) interstellar chemistry. In hot carbon-rich circumstellar shells, for example, the dominant chemical pathway to the formation of PAHs and hydrocarbons is the successive addition of C_2H_2 [*Allamandola1989*]. Similar processes are assumed and investigated under the condition of the interstellar ultra-low densities and temperatures [*Smith1992, Millar1997*].

Under constraints of high unsaturation and charged states of hydrocarbons some mechanisms still work (see reaction rates of [*Millar1997*]), but the addition of C_2H_2 to (charged) PAHs show distinctive reaction barriers. Without the proper photo-induced activation, like in the case of dark clouds, C_2H_2 additions are not favoured.

One of the aims of this project was to study growth mechanisms for PAHs and analogues from highly abundant interstellar species. Under the constraints imposed by the ISM, the molecular growth reactions are supposed to be dominated by binary gas-phase collisions.

In order to study dynamic effects of collisions, we focused on the calculations of collision trajectories. However, static calculations were considered for the analysis of important molecular states, such as transition states or local minima. The collision trajectory calculations were based on a quasi-classical molecular dynamics (MD) approach combined with Density-Functional Theory (DFT) methods [*Harris1985*]. To sample the potential energy surface (PES) of collisions within a statistical framework, we used the Density-Functional Tight-Binding (DFTB) method. This method provides superior computational efficiency and also reasonable accuracy. The characteristic mechanisms of single reaction channels were solved by the nudged elastic band method (NEB). The properties of the reactants and the products, as well as the intermediates and the transition states of the reaction channels, were refined by modest levels of quantum chemistry methods, e.g. post-Hartree-Fock methods.

3.4 Angewandte Methoden / Experimental methods

Quasi-classical trajectories to sample the potential energy surface (PES)

The approach to study large reaction systems, without a reaction PES parameterisation, is based on earlier works by Seifert and Porezag [*Seifert1996, Seifert1992, Porezag1995*]. Under the adiabatic approximation, molecular dynamic trajectories $R_i(t)$ can be obtained by solving the coupled set of Newton-type equations,

$$M_i \ddot{R}_i = \frac{\partial}{\partial R_i} E(R_1, \ldots, R_N)$$

where N represents the number of nuclei with masses Mi (i=1,...,N) and E(R1,...,RN) represents the energy of the electronic ground state of the Born-Oppenheimer surface. The energies are calculated by the DFTB method [*Seifert1996, Porezag1995, Seifert1992*].

The above set of equations of motion is integrated numerically by a Verlet algorithm. To fulfil the total energy conservation condition, the time step for all quantum MD simulations was restricted to 10 a.u.

Each collision trajectory between the two reactants was started at a quasi interaction-free distance. After the collision or the point of minimal encounter, the trajectories were propagated for a further timer interval of 6 picoseconds (ps). Additionally, the total momentum of the collision system was considered to be conserved.

The statistics were set up by randomisation of the initial trajectory conditions (such as relative orientation). The impact parameter ***b*** was varied systematically, allowing the calculation of the capture cross section σ by integrating the capture/reaction probabilities ***P(b)*** over the impact parameter **b**. To achieve a representative integration over the reaction probabilities, 50 to 100 trajectories had to be propagated for each range of impact parameter ($\Delta \boldsymbol{b} < 0.4$ a.u.). This high number of calculated trajectories also guaranteed a good sampling of the local reaction potential energy surface as well as a pre-selection of important reaction channels. Finally, thermal rate coefficients ***k(T)*** were derived from the proper average $\langle \sigma(\varepsilon)\varepsilon \rangle$.

Minimum energy path (MEP) calculations of reaction channels (RCs)

The lowest reaction paths corresponding to pre-selected reaction channels were refined and re-optimised using the NEB method [*Henkelman2000, Henkelmann2000a*]. Chain-of-state methods, such as NEB, allow a search of transition states (TS) between unconnected local minima on the reaction PES. The optimisation to the MEP by the NEB method follows a force projection scheme:

$$F_i = F_i\big|_{\|} - \nabla E(R_i)\big|_{\perp}$$

Forces and total energies were computed in combination with the DFTB (DeMon package [*Köster2004*]) and with the B3LYP method (Gaussian package [*Frisch2004*]).

Comparison of different approaches

In addition, the geometry of reactants, product isomers as well as intermediates and transition states of importance were re-optimised using the hybrid B3LYP method. For the optimization and the analysis of the harmonic frequencies we have used B3LYP in the 6-31G(d) basis set. Total energy values were refined by single point calculations with larger basis sets such as 6-311++G(3df,3pd). Furthermore, results were compared with post-Hartree-Fock methods such as G3 [*Curtiss1998, Baboul1999*] and MP2. Finally, the harmonic frequency analysis was revised at MP2/6-31G(d) level. For all calculations the Gaussian quantum chemistry package was used.

3.5 Ergebnisse und ihre Bedeutung / Results and their importance

Reactions of interstellar hydrocarbons with methylidine (CH)

a) monocyclic hydrocarbons

Reactive collisions of methylidine with different hydrocarbons were studied in order to check the suitability of methylidine as a precursor of hydrocarbon growth under the constraints of the ISM. Photochemical processes were not considered.

CH addition at arbitrary hydrocarbon positions was found to release of a high amount of reaction energy (5-8 eV). This fact can be related to the trivalent and strong electron donating character of the CH molecule. Its three valence electrons allowed the formation of three new bonds.

CH addition to monocyclic hydrocarbons can lead to an extension of the ring. The results of the CH ring extension of $C_xH_y^+$ are summarized in Table 1 (corresponding structures are shown in Fig. 1).

Table 1: Reaction energies in eV. Isomers are taken from Fig. 1.

X + CH → Y	DFTB	B3LYP	G3
α-$C_5H_5^+$, α-$C_6H_6^+$	-7.3710	-7.7536	-7.2775
α-$C_6H_6^+$, α-$C_7H_7^+$	-6.1458	-7.3951	-7.0827
α-$C_7H_7^+$, α-$C_8H_8^+$	-4.6859	-4.3160	-4.2443
α-$C_8H_8^+$, α-$C_9H_9^+$	-5.8525	-5.8260	-6.1804
α-$C_9H_9^+$, α-$C_{10}H_{10}^+$	-6.1156	-5.4932	-

Information about the product distribution was obtained by an analysis of the reactions between $C_xH_x^+$ and CH. Thermodynamic properties of important products were investigated (see Fig.1).

Table 2: Capture rate constants at 100 K and canonical capture cross sections at total collision energy of 0.01 eV.

X + CH → Y	$k_{100\,K}/10^{-10}cm^3s^{-1}$	$\sigma_{0.01\,eV}/10^{-20}m^2$
α-$C_5H_5^+$, α-$C_6H_6^+$	6.3	181.0
α-$C_6H_6^+$, α-$C_7H_7^+$	6.1	180.1
α-$C_7H_7^+$, α-$C_8H_8^+$	6.9	206.5
α-$C_8H_8^+$, α-$C_9H_9^+$	7.7	222.6
α-$C_9H_9^+$, α-$C_{10}H_{10}^+$	8.4	239.4

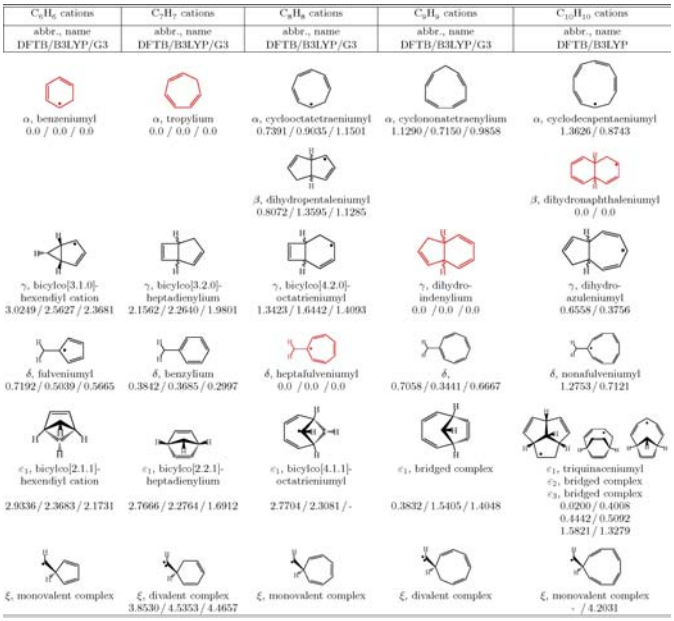

Fig. 1: Products of the reaction $C_xH_x^+$ + CH to $C_{x+1}H_{x+1}^+$ (x=5-9). The first row shows the monocyclic products (α), second (β) and third row (γ) show the even and uneven sized bicyclic fused ring products. The fourth row (δ) sketches fulvene derivates, the fifth row (ε_i) bridged polycyclic fused ring isomers whereas the last row (*A*) shows intermediate structures of initial association. For convenience, the hydrogen atoms of sp^2 hybridised carbon atoms are not shown. Relative total energies of products are given at the SCC-DFTB, B3LYP/6-311++G(3df,3pd)//B3LYP/6-31G(d) and G3 level, respectively.

Due to the absence of an entry barrier, almost the entire low-energy collisions were reactive. The cross sections and rate constants of the reactions were found to be close to the capture values of the Langevin model (Table 2.). The results will be described elsewhere in more detail [*Barthel2007a*].

Zero-point vibration, entropy, and enthalpy corrections of the products were calculated at different temperatures in order to calculate the product distribution/population in thermodynamic equilibrium. The basics of population calculations were described elsewhere in more detail [*Slanini2003*]. Our results for temperatures ranging between 0 and 5000 K are shown in Fig. 2, revealing that up to 1000 K the product distribution is dominated by the most stable isomers (Fig. 1).

As a function of the number of carbon atoms (and of ring size), the most stable reaction product changes from monocyclic isomers of $C_6H_6^+$ and $C_7H_7^+$ systems (solid lines in Fig. 2), over methylidene structures of $C_8H_8^+$ systems (dashed lines) to bicyclic structures of $C_9H_9^+$ and $C_{10}H_{10}^+$ system (dotted lines). Except for the $C_8H_8^+$ reaction system, the energetic estimates agree with the product distribution of the MD simulations.

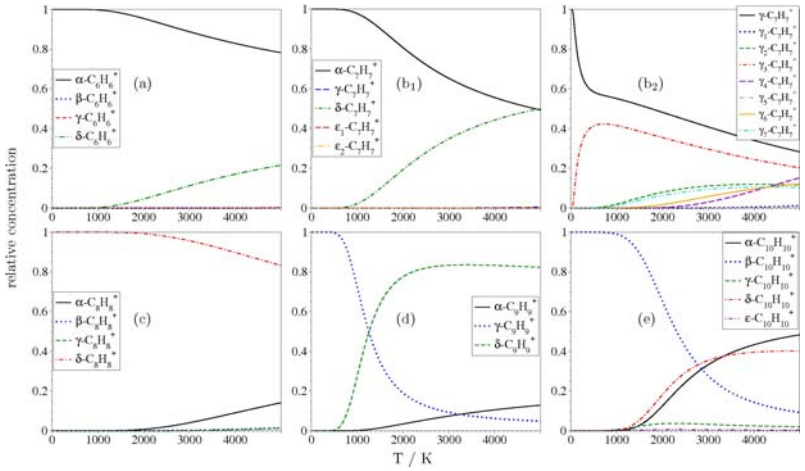

Fig. 2: Population analysis of products of the reactions $C_xH_y^+$ + CH to $C_{x+1}H_{y+1}^+$: a) x=5 b_1) x=6 b_2) x=6 (different γ-isomers) c) x=7 d) x=8 and e) x=9 at the B3LYP/6-311++G(3df,3pd)//B3LYP/6-31G(d) level

The origin of the product distribution found by MD simulations and the formation of bicyclic bridged and fused ring systems (see β- and γ-isomers of Fig. 1) were studied by reaction channel mechanisms. The NEB method was used in combination with DFTB and B3LYP methods. The successive formation of polycyclic isomers was found to be a feature of the CH electron trivalence. The first order association products (*A*-isomers of Fig. 1) were observed to form further bonds. The reaction dynamics often forced the formation of a second bond with non-adjacent carbon atoms. This led to the formation of the ε-isomers (Fig. 3).

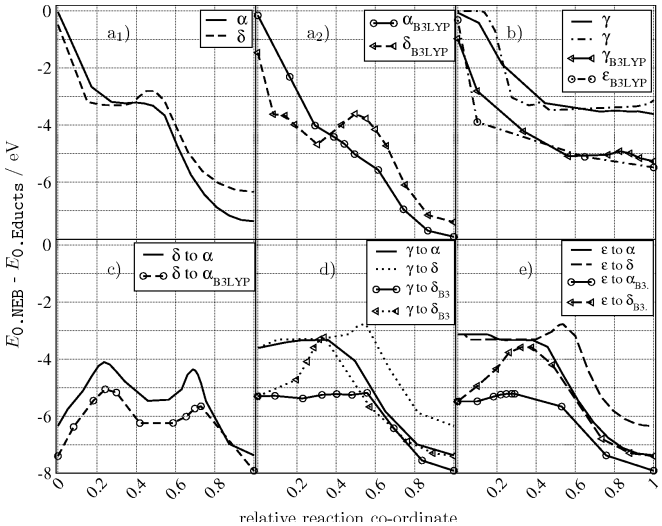

Fig. 3: Reaction channels in a_1) and a_2) represent the association of α-$C_6H_6^+$ and δ–$C_6H_6^+$, b) the associations of γ–$C_6H_6^+$ and ε–$C_6H_6^+$. In c), d) and e) isomerisations of all isomers into each other are shown. The reference point is set to α–$C_5H_5^+$ + CH.

In Fig. 3, the different mechanisms for the formation and depletion of the $C_6H_6^+$ isomers are shown. Certain aspects of the formation and stability / depletion of isomers were found to repeat independently of the system size. The formation of the δ-isomers was found to be always hindered due to a common reaction barrier. For reaction systems $C_xH_x^+$ + CH with x=8-9, the formation of the δ-isomers was not observed. The barrier-less reaction channels with broad entrances on the potential energy surface were often found to suppress the δ-isomer channel. The α- and some ε-isomer channels were found to be barrier-less [*Barthel2007a*].

The reaction energy can be dissipated in the form of molecular dissociation. In particular, dissociation channels of molecular hydrogen (H_2) and acetylene (C_2H_2) were investigated. The latter dissociation channels were occasionally observed (fraction less than 1/100 within 6 ps) for systems such as $C_xH_x^+$ + CH with x=8,10. A dissociation channel producing H_2 was not found. However, the study of such dissociation channels indicated that bicyclic isomers of $C_9H_9^+$ and $C_{10}H_{10}^+$ have a high tendency to lose H_2. On the other hand, bicyclic systems of $C_7H_7^+$ and $C_8H_8^+$ were found to have high barriers for H_2-dissocation (Fig. 4).

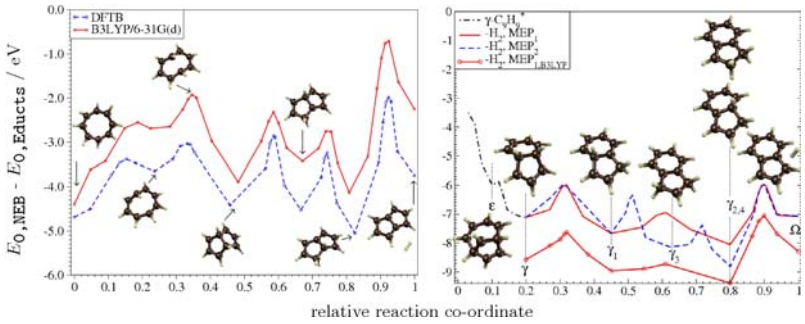

Fig. 4: H_2 dissociation channels of the bicyclic β-$C_8H_8^+$ and γ-$C_9H_9^+$.

Based on these results, we can conclude that the addition of CH to monocyclic hydrocarbons leads to extended ring structures and transformation of monocyclic ring to bicyclic rings, so that it can lead to reaction channels for the formation of aromatic fused ring structures (naphthalene, indene).

The very high energetic impact of reactions with CH could produce radiative emission features similar to processes that follow UV absorption. Therefore, observed interstellar IR-emission features could also be assigned to chemical reactions.

b) bicyclic hydrocarbons

The study of CH addition reactions was extended to larger hydrocarbon molecules in order to develop a general reaction scheme for growth of polycyclic aromatic hydrocarbons. The pathway from naphthalene to phenanthrene was investigated (Fig. 5).

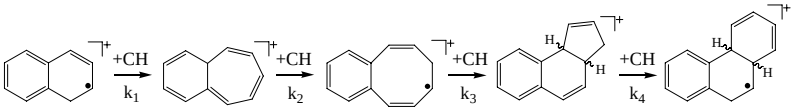

Fig. 5: Reaction path of naphthalene to 4a,10a-dihydrophenanthrene.

Investigations about the reaction energetics and the MD aspects are summarized in Table 3 and Table 4.

Table 3: Reaction energies in eV. Isomers are taken from Fig. 5.

X + CH -> Y	DFTB	B3LYP	MP2
α-$C_{10}H_8^+$, α-$C_{11}H_9^+$	-6.1369	-6.6199	-7.3086
α-$C_{11}H_9^+$, α_1-$C_{12}H_{10}^+$	-4.9606	-4.5902	-
α_1-$C_{12}H_{10}^+$, α_1-$C_{13}H_{11}^+$	-6.0782	-6.7278	-
γ_1-$C_{13}H_{11}^+$, α_1-$C_{14}H_{12}^+$	-6.1661	-5.9271	-

Table 4: Canonical capture cross sections at 0.01 eV total collision energy and capture rate constants at 100 K.

X + CH -> Y	$k_{100\,K}/10^{-10}cm^3s^{-1}$	$\sigma_{0.01\,eV}/10^{-20}m^2$
α-$C_{10}H_8^+$, α-$C_{11}H_9^+$	8.43	240.2
α-$C_{11}H_9^+$, α_1-$C_{12}H_{10}^+$	7.56	237.9
α_1-$C_{12}H_{10}^+$, α_1-$C_{13}H_{11}^+$	9.39	260.1
γ_1-$C_{13}H_{11}^+$, α_1-$C_{14}H_{12}^+$	9.35	264.3

The product distribution of all reactions is depicted in Fig. 4. The product variety was found to be increased compared to monocyclic hydrocarbons, simply by the increase of positions that can be attacked by CH.

It was found that tri- and tetracyclic structures are easily formed either by transformation of bridged product structures or via intermediates with extended ring structures. The methylenyl substituted isomers (δ isomers of Fig. 1) were not formed within the applied simulation time of 6 ps, in agreement with the study of monocyclic hydrocarbons.

Despite CH addition reactions, we observed in particular H abstraction reaction of the kind $C_xH_{x-3}^+ + CH_2$ or $C_xH_{x-4}^+ + CH_3$. It was found that weakly bound H atoms of sp^3 hybridised carbon atoms, in particular at bridging positions, were most efficient in transferring hydrogen to the CH molecule. These reaction channels are

highly exothermic and lead to aromatic systems. Additionally, the H transfer to CH was most efficient in cases where the CH insertion is sterically hindered.

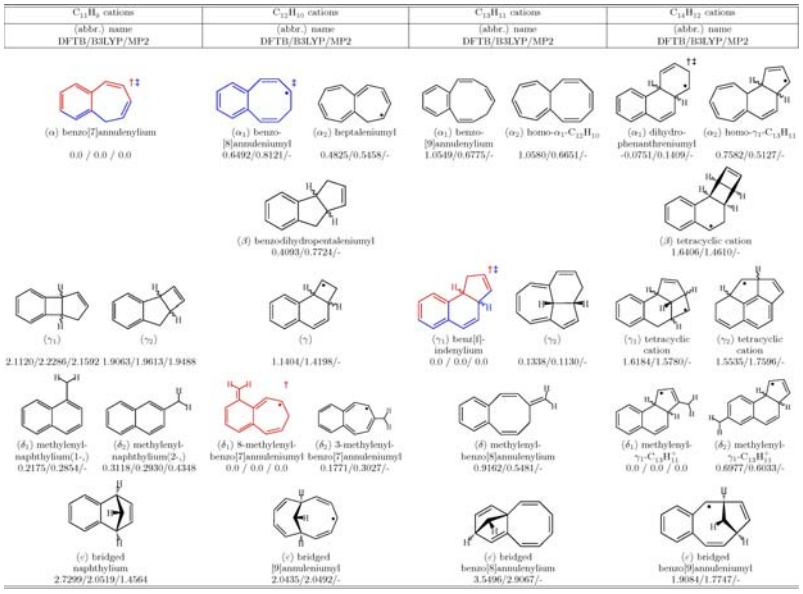

Fig. 6: Products of the reaction $C_xH_{x-2}^+$ + CH to $C_{x+1}H_{x-1}^+$ (x=10-13). The first row (α) shows products of ring extension, second (β) and third row (γ) products of ring constriction (new ring condensation), the fourth row (δ) methylene derivatives whereas the fifth row (ε_i) shows monovalent metheno-bridged polycyclic isomers. Total energies of products at SCC-DFTB, B3LYP/6-311++G(3df,3pd)//B3LYP/6-31G(d) and MP2/6-31G(d) level are reported with respect to the most stable isomer.

c) polycyclic hydrocarbons

Reactions of CH with large fused polycyclic hydrocarbon were studied from the point of view of peripheral vs. centred attack as well as steric hindrances. Three different reaction systems were considered (see first row of Fig. 7. The reaction energies (0 K) are given in Table 5.

The reactions of both $C_{20}H_{10}^+$ isomers with CH were highly exothermic and resulted in ring expansion. Ring expansion of $C_{24}H_{12}^+$ releases less energy due to an increase of tension inside the molecular system during the expansion process.

The stability of first order association products (A_{Xj}, last row of Fig. 7) depends on the geometric configuration. It was found that CH attachment at a peripheral pentagon results in ring extension without any reaction barrier. However, at centred pentagons, such as in corannulene, insertion or bridging was found to exhibit significant barriers. Peripheral hexagon ring extension was found to have barriers below 0.5 eV. The bridging and extension of interior hexagons had barriers above 1 eV.

Table 5: Reaction energies in eV. Isomers are taken from Fig. 1.

X + CH -> Y	DFTB	B3LYP
$C_{20}H_{10}^+$(a), α_{A1}-$C_{21}H_{11}^+$	-7.5527	-7.5771
$C_{20}H_{10}^+$(b), α_{B1}-	-7.1379	-7.8004
$C_{24}H_{12}^+$, α_1-$C_{25}H_{13}^+$	-5.7679	-

Table 6: Canonical capture cross sections at 0.01 eV total collision energy and capture rate constants at 100 K.

X + CH -> Y	$k_{100\,K}/10^{-10}cm^3s^{-1}$	$\sigma_{0.01\,eV}/10^{-20}m^2$
$C_{20}H_{10}^+$(a), α_{A1}-$C_{21}H_{11}^+$	11.6	313.7
$C_{20}H_{10}^+$(b), α_{B1}-	10.5	312.8
$C_{24}H_{12}^+$, α_1-$C_{25}H_{13}^+$	12.5	343.3

Additionally, it was found that the CH is often weakly bound and drifts towards the periphery during the MD simulations. This was also noticed for the $C_{25}H_{13}^+$ system. We conclude that despite an attack of CH at

arbitrary molecular positions, the systems grow in the periphery. In particular, the ring extension will follow the growth scheme of mono- and bicyclic hydrocarbons. Further implications for the reaction mechanisms will be discussed elsewhere [*Barthel2007a*].

Reactions of interstellar aromatic hydrocarbons with di- and trivalent polyatomic reactants

Within the project, the suitability of small polyatomic molecules as precursors for hydrocarbon growth mechanisms was investigated in detail. Reactant candidates were selected according to their interstellar abundances. A further pre-selection of suitable candidates was deduced from our own MD calculations of the respective reactivity. The final scheme for the growth process was designed by various combinations of the selected precursors. An overview of the investigated systems is depicted in Fig. 8.

Collisions of non-activated aromatic hydrocarbon cations with C_2H_2 (acetylene) were mostly non-reactive whereas for substituted and activated aromatic species a moderate reactivity with acetylene was found. We conclude that acetylene plays only a minor role for hydrocarbon growth at temperatures below 50 K. Further details can be found in a forthcoming publication [*Barthel2007c*].

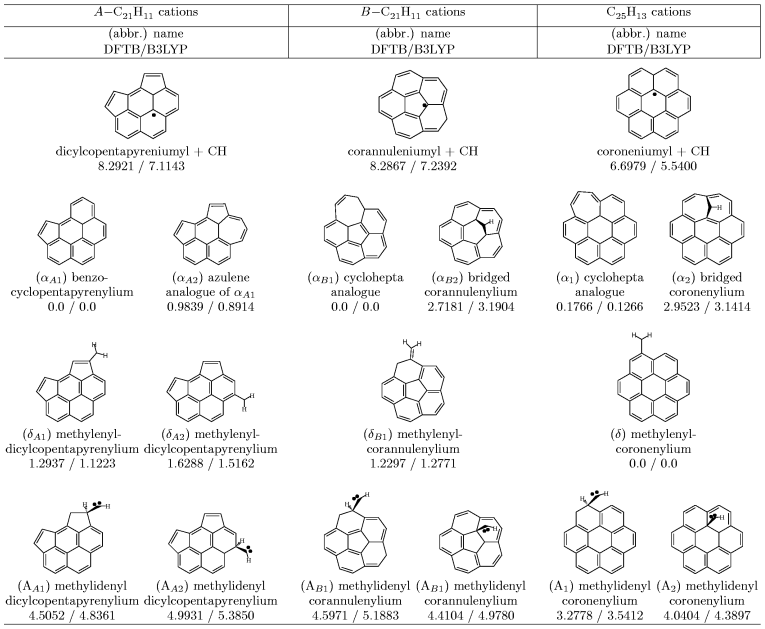

Fig, 7. Products of the reaction $C_xH_{x/2}^+$ + CH to $C_{x+1}H_{x/2+1}^+$ (x=20,24). The first row shows the educts + CH, the second row (α) products of ring extension and ring bridging, the third row (δ) methylene derivatives whereas the fourth row (e_i) shows the first order association products. Total energies of products at SCC-DFTB, B3LYP/6-311++G(3df,3pd)/ /B3LYP /6-31G(d) and MP2/6-31G(d) level are reported with respect to the most stable isomer.

High reactivity at very low temperature was obtained from reactions between non-activated hydrocarbons and small molecules with multiple electron valences such as cummulene carbenes and derivatives, in particular H_2C_2 (vinylidene), H_2C_3, H_2C_4 and C_3H.

a) Reactions with C_3H

The studies of C_3H-based reactions include a complete set of growth reactions from $C_7H_7^+$ to $C_{14}H_{10}^+$ (see right part of Fig. 9). The analysis of the MD simulations is given in Table 7. It was found that under a suitable orientation of the reactants the addition of C_3H pass through a barrier-less channel. However, ring condensations (e.g. hexagons at 3-carbon bays) were connected with reaction barriers which were found to be smaller than the total amount of released reaction energy (see Fig. 9).

Despite the electron trivalence of C_3H, the addition rates at ring structures were found to be moderate compared with the trivalent CH based reactions. A substituted hydrocarbon ring such as δ-$C_7H_7^+$ was found to show a higher reactivity than α-$C_7H_7^+$. Additionally, non-substituted ring structures such as tropylium (α-$C_7H_7^+$) and naphthalene cations were found to have large deviations between the capture and association based reaction cross sections. This phenomenon is caused by the formation of H-bridged and orbiting complexes.

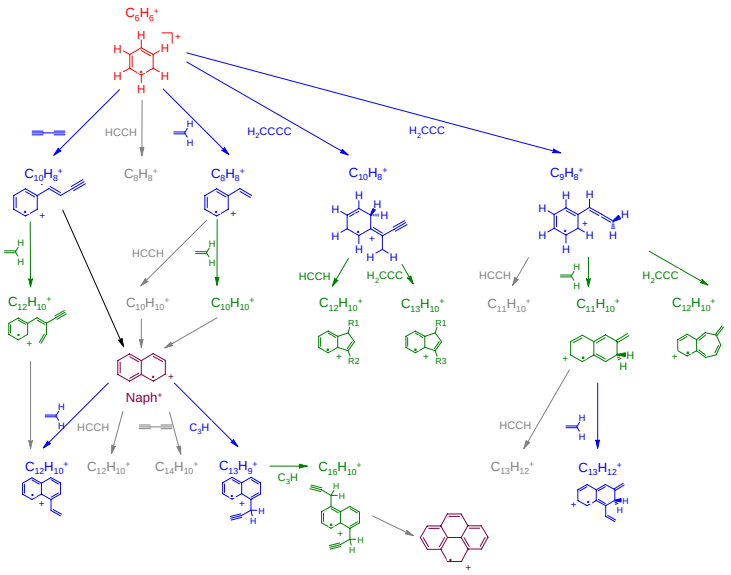

Fig. 8: Schematic overview of investigated reaction system of hydrocarbons with not-valent reactants such as C_2H_2 as well as with divalent and trivalent reactants such as H_2C_2, H_2C_3, H_2C_4 and C_3H.

It was found that under a suitable orientation of the reactants the addition of C_3H pass through a barrier-less channel. However, ring condensations (e.g. hexagons at 3-carbon bays) were connected with reaction barriers which were found to be smaller than the total amount of released reaction energy (see Fig. 9).

Table 7: Reaction cross sections at 0.01 eV total collision energy and reaction rate constants at 100 K evaluated after 6 ps simulation (t_0=initial collision hit). Values of the capture process are given in brackets.

X + C_3H -> Y	$k_{100\,K}/10^{-10}cm^3s^{-1}$	$\sigma_{0.01\,eV}/10^{-20}m^2$
α-$C_7H_7^+$, α-$C_{10}H_8^+$	1.509 (5.562)	67.2 (244.3)
δ-$C_7H_7^+$, α-$C_{10}H_8^+$	4.348 (6.460)	182.6 (266.0)
α-$C_{10}H_8^+$, α-$C_{13}H_9^+$	2.276	98.0
α-$C_{13}H_9^+$, α-$C_{16}H_{10}^+$	2.987	125.8

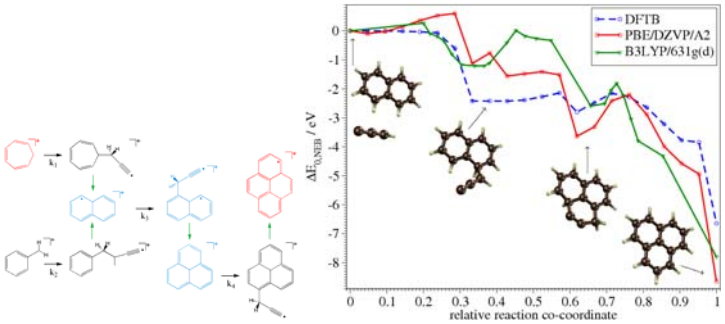

Fig. 9: Left: formation path with C_3H precursor, right: addition of C_3H to $C_{10}H_8^+$ and ring closure mechanisms of the product.

b) Reactions with H_2C_2, H_2C_3 and H_2C_4

H_2C_2 (vinylidene) based collisions with non-activated aromatic hydrocarbons cation, such as benzene and naphthalene, were studied. The activated products as well as products of other cummulene carbenes were exposed to further collision reactions with H_2C_2 (Fig. 8), resulting in a high reactivity for H_2C_2 addition to hydrocarbons. Inelastic scattering of H_2C_2 often triggered an isomerisation to acetylene. The analysis showed that a ring condensation requires at least 2 H_2C_2 addition steps. However, the low selectivity of H_2C_2 did not favour ring condensation. Without activated sidegroups (such as allenyl groups), the growth with a H_2C_2 precursor leads to tree-like structures rather then ring fused structures.

H_2C_3 and H_2C_4 based collisions with aromatic hydrocarbons cations were found to be dominated by the formation of cummulenyl sidegroups. High ring closure barriers were obtained which hinder cummulenyl

sidegroups undergo ring condensation. However, after H_2C_2 addition, cummulenyl can condensate to 6-membered rings.

Reactions of interstellar hydrocarbons with non-valent polyatomic molecules

In this project, we also investigated the ability of non-valent precursors to induce growth of hydrocarbons at ultra-low temperature.

a) C_4H_2

Condensation reactions with diacetylene and (poly)aromatic hydrocarbon cations were investigated, including a detailed analysis of the products with respect to ring condensation processes of the sidegroups. Barriers for rotation and ring closure (see Fig. 10) were found to be reduced due to the charged state. Moreover, the released reaction energy is sufficient for providing the required internal motion. More implications were discussed elsewhere [*Barthel2003*].

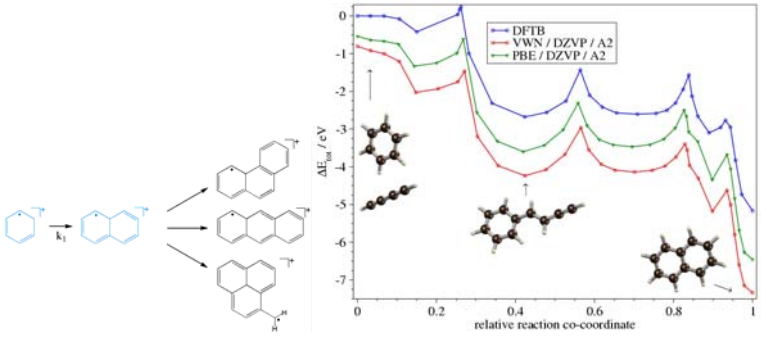

Fig. 10: Left: formation path with C_4H_2 precursor, right: addition of C_4H_2 to $C_6H_6^+$ and ring closure mechanisms of the product.

c) C_3H_3 (allyl) cations

The possibility to obtain ring condensation from the addition of the allyl cation to small hydrocarbons was investigated, in particular the formation of benzene. According to the reviews by [*Smith1992*, *Millar1997*], a single step addition of an allyl cation to C_3H_4 should lead to benzene. Collision MD simulations were performed for two isomers of C_3H_4: Allene and methylacetylene. Reactive collisions with allene were found to result in cyclisation within less than 3.5 ps. In contrast, for methylacetylene, no cyclisation of the reaction products was found. The calculations of the reaction path are depicted in Fig. 11.

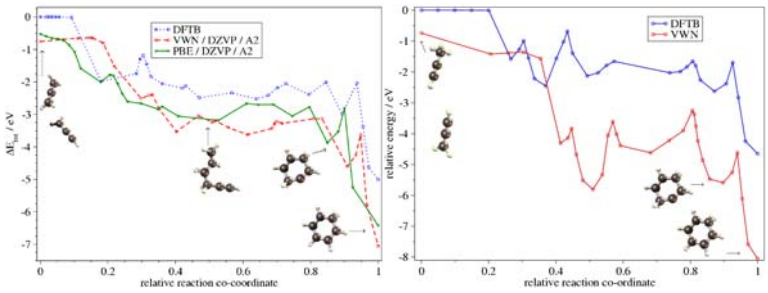

Fig. 11: Ring formation process by two different processes: a) $C_3H_3^+ + H_2CCCH_2$ b) $C_3H_3^+ + H_3CCCH$

Reactions of hydrocarbons with tetravalent C_2

In collaboration with the group of C. Joblin, France, we have investigated the formation and the photoinduced oxidation of coronone ($C_{24}H_{12}^+$) and its derivatives.

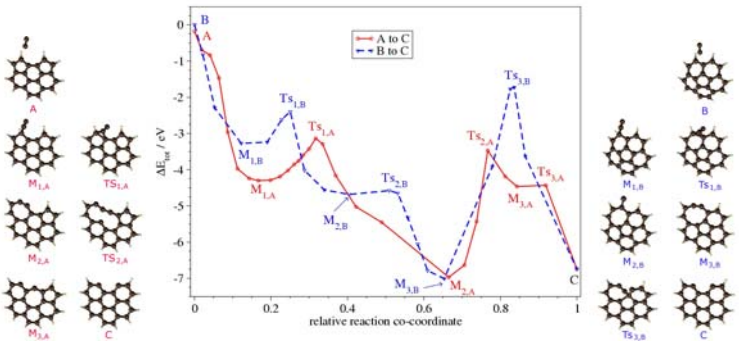

Fig. 12: C_2 addition reaction with dicyclopentapyrene cation (right, red solid line) and corannulene cation (left, blue dashed line) at PBE/DZVP level.

In particular, the mechanisms of C_2 and CO fragmentation during the photoinduced oxidation of coronene was studied [*Barthel2007b*]. Additionally, a retrosynthesis by C_2 addition reactions was sketched. Pathways of the reorganisation of the C_2-addition products are shown in Fig. 12.

Excited states of C_3

In this part of the project, it was demonstrated that the lowest excited state of C_3 is a triplet state in the geometry of an equilateral triangle, compare the FGLA report 2000 – 2003. By applying time-dependent density functional theory (TD-DFT) to the lowest singlet and triplet states, we have mapped the lowest single-electron excitations up to an energy of about 10 eV above each initial state.

As an example for the results obtained in a comprehensive study of the lowest excited states of C_3 [*Terentyev2004*], we report the lowest triplet states obtained via excitations from the singlet ground state (Fig. 13) and from the lowest triplet configuration at large bond angles (Fig. 14).

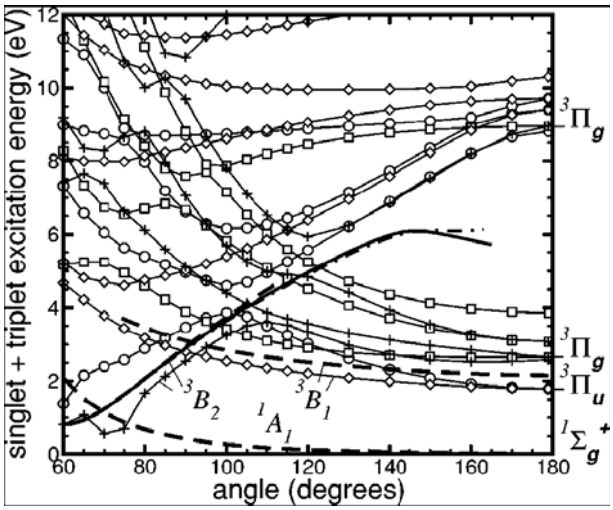

Fig. 13: Total energy of the lowest triplet states, calculated as the sum of the B3LYP/6-31G(d) energy of the singlet ground state with optimized bond length and the B3LYP/6-31G(d) TD-DFT excitation energies. Total energy curves resulting from calculations based on B3LYP/6-31G(d) (dashed), QCISD/6-311G(d) (solid) and QCISD/6-311+G(d) (dot-dashed) are included for comparison. Symbols: circles $^3A_1$; squares $^3A_2$, diamonds $^3B_1$, crosses $^3B_2$.

In order to assess the total energy of the lowest triplet states, we add the energy of the singlet ground state and the triplet excitation energies calculated with TD-DFT, Fig. 13. For linear C_3, the calculated excitation energy of the triplet energy is 1.8 eV, giving an estimate of about -0.35 eV for systematic deviations between the TD-DFT excitation energies and a total energy calculation excluding corrections due to zero point motion. As can be seen from the low-energy region of Fig. 13, this systematic deviation for the lowest triplet of $^3B_1$ symmetry does not depend much on the bond angle. For bond angles below 90°, the deviation between the TD-DFT result and the total energy of the lowest $^3B_2$ triplet is somewhat larger, including some scatter close to the inter-system crossing around 70°. Interestingly, for linear C_3 the calculated difference of 0.86 eV between the two lowest triplet states $^3\Pi_u$ and $^3\Pi_g$ is in good agreement with the experimental value of 0.80 eV [*Sasada1991, Tokaryk1995*].

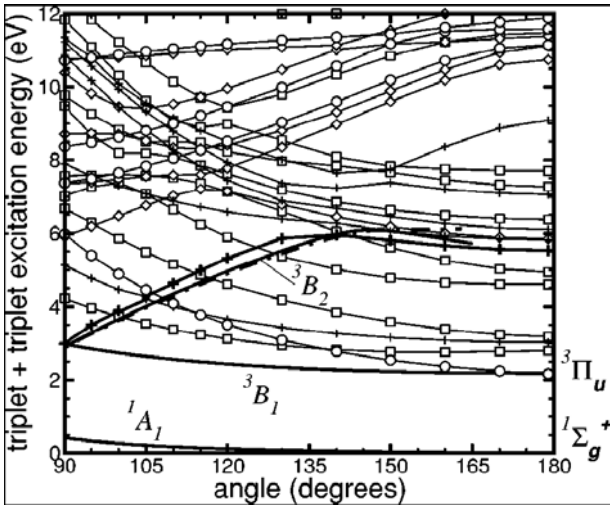

Fig. 14: Total energy of the lowest triplet states, calculated as the sum of the B3LYP/6-31G(d) energy of the lowest $^3B_1$ triplet state with optimized bond length and the B3LYP/6-31G(d) TD-DFT excitation energies to higher lying triplets. The total energy curves of the B3LYP/6-31G(d) calculation for the $^1A_1$ singlet and the $^3B_1$ triplet are superimposed (solid line). The total energy curves of the QCISD calculations of the $^3B_2$ triplet (thick lines) are included for comparison, based on the 6-311G(d) (solid) and 6-311+G(d) (dash-dotted) variational basis sets. The lowest $^3B_2$ triplet state is highlighted with heavy symbols. Symbols are defined as in Fig. 13.

Triplet energies defined by excitations starting from the $^3B_1$ triplet ground state are shown in Fig. 14. As the starting electronic configuration $^3B_1$ contains already two unpaired electrons, three kinds of excitations can occur. First, excitations between different valence states will result in low-lying excitations between different triplet configurations. Second, one of the remaining 7 electrons in the four highest occupied valence states can be promoted into a virtual orbital, resulting in electronic configurations which cannot be reached via a single excitation out of the singlet ground state. The third possibility is an excitation of the unpaired electron in the LUMO into higher virtual orbitals, resulting in some of the triplet states displayed in Fig. 13. Nevertheless, these excitations of a single electron starting from the triplet ground state still do not cover all the excited states, as some double excited are still excluded.

These TD-DFT investigations give a comprehensive map of all the low-lying states of C_3 which can be reached via single excitations from the singlet or triplet ground states. However, due to restrictions in the final configurations, some states in the energetic range of interest cannot be reached.

3.6 Zusammenfassung und Ausblick / Summary and future

In this project, ultra-low temperature based growth processes of hydrocarbons with various kinds of precursors were investigated. The precursors were selected according to the known interstellar abundances and reactivities based on previous calculations. The investigated reaction mechanisms provide new insight into growth processes of PAHs in interstellar objects such as dense clouds. The results also strengthen the PAH hypothesis. Calculated cross sections and rate coefficients are a useful support for calculation-based modelling of interstellar chemical reaction networks.

The results and the comparison with DFT and post-Hartree-Fock methods demonstrate that the DFTB in combination with quantum MD simulations and NEB calculations are very useful methods to study reactions dynamics and mechanisms. DFTB based results are applicable for B3LYP and post-Hartee-Fock based calculations. As a perspective for future work, the good qualitative agreement between DFTB and B3LYP/post-Hartree-Fock based results opens up new strategies for reliable studies of very large reaction systems. Formation of hydrogenated amorphous carbon (HAC) and formation of soot or fullerene will be candidates of investigation.

3.7 Literatur / References

Allamandola, L. J., Tielens, A. G. G. M., Barker, J. R. *Polycyclic aromatic-hydrocarbons and the unidentified infrared-emission bands – auto exhaust along the milky-way*, Astrophys. J. **290** (1985), L25.

Allamandola, L.J., Tielens, A.G.G.M., Barker, J.R., *Interstellar polycyclic aromatic-hydrocarbons infrared-emission bands, the excitation emission mechanism, and the astrophysical implications*, Astrophys. J. Suppl. Series**, 71** (1989), 733.

Baboul, A. G., Curtiss, L. A., Redfern, P. C., Raghavachari, K., *Gaussian-3 theory using density functional geometries and zero-point energies*, J. Chem Phys., **110** (1999), 7650.

Bakes, E. L. O., Tielens, A. G. G. M. *The photoelectric heating mechanism for very small graphitic grains and polycyclic aromatic-hydrocarbons*. Astrophys. J. **427** (1994), 822.

Barthel, R.: *Theoretische Untersuchung zur Bildung von Kohlenwasserstoffen unter astrophysikalischen Bedingungen*, Master Thesis, Technische Universität, (2003).

Barthel, R.: *Computational study of interstellar hydrocarbon formation*, Ph.D. Thesis, Technische Universität, (2007), under preparation.

Barthel, R., Scholz, R., Seifert, G.: *Growth mechanisms of interstellar polycyclic hydrocarbons: reactions with methylidine*, Astron. Astrophys. (2007a), under preparation.

Barthel, R., Heine, T., Joblin, C., Seifert, G.: *Photoinduced dissociation of hydrocarbons: coronene, corannulene and isomers*, (2007b), under preparation.

Barthel, R., Seifert, G.: *Growth mechanism of interstellar polycyclic hydrocarbons: reactions with di- and trivalent polyatomic molecules*, Astron. Astrophys. (2007c), under preparation.

Brechignac, P., Schmidt, M., Masson, A., Pino, T., Parneix, P., Brechignac, C., *Photoinduced products from cold coronene clustersa route to hydrocarbonated nanograins?* Astron. Astrophys. **442** (2005), 239.

Curtiss, L. A., Raghavachari, K., Redfern, P. C., Rassolov, V., Pople, J. A., *Gaussian-3 (G3) theory for molecules containing first and second-row atoms*, J. Chem. Phys. **109** (1998), 7764.

Duley, W. W., Williams, D. A., *The infrared-spectrum of interstellar dust surface functional-groups on carbon.*, Mon. Not. Roy. Astron. Soc. **196** (1981), 269.

Fischer, G., Barthel, R., Seifert, G. *Molecular dynamics study of the reaction C_3+H_3^+*, Eur. Phys. J. D **35** (2005), 479.

Frisch, M.J., et al., *Gaussian 03, Rev. C.02*, Gaussian, Inc., Wallingford CT, USA,

Habart, E., Verstraete, L., Boulanger, F., des Forets, G. P., Le Peintre, F., Bernard, J. P., *Photoelectric effect on dust grains across the L1721 cloud in the rho Ophiuchi molecular complex*, Astron. Astrophys. **373** (2001), 702.

Harris, J. *Simplified method for calculating the energy of weakly interacting fragments*, Phys. Rev. B **31** (1985), 1770.

Henkelman, G., Jonsson, H. *Improved tangent estimate in the nudged elastic band method for finding minimum energy paths and saddle points*. J. Chem. Phys. **113** (2000), 9978.

Henkelman, G., Uberuaga, B. P., Jonsson, H. *A climbing image nudged elastic band method for finding saddle points and minimum energy paths.* J. Chem. Phys. **113** (2000a), 9901.

Jones, A. P., Tielens, A. G. G. M., Hollenbach, D. J. *Grain shattering in shocks: The interstellar grain size distribution*, Astrophys. J. **469** (1996), 740.

Köster A.M., et al., *deMon 2003, Ver. 1.1.0*, The National Research Council, Ottawa, Canada (2004).

Leger, A., Dhendecourt, L., Defourneau, D. *Physics of ir emission by interstellar pah molecules*, Astron. Astrophys **216** (1989), 148.

Leger, A., Puget, J. L. *Identification of the unidentified ir emission features of interstellar dust*, Astron. Astrophys **137** (1984), L5.

Millar, T. J., Farquhar, P. R. A., Willacy, K.: *The UMIST database for astrochemistry 1995*, Astron. Astrophys. Suppl. Series **121** (1997), 139.

Perez, N., Heine, T., Barthel, R., Seifert, G., Vela, A., Mendez-Rojas, M., Merino, G., *Planar tetracoordinate carbons in cyclic hydrocarbons*, Org. Lett. **7**, (2005) 1509.

Porezag, D., Frauenheim, T., Kohler, T., Seifert, G., Kaschner, R. *Construction of tight-binding-like potentials on the basis of density-functional theory application to carbon.* Phys. Rev. B **51** (1995), 12947.

Sasada, H., Amano, T., Jarman, C., Bernath, C.P., *A new triplet band system of C_3: The $b^3\Pi_g$ - $a^3\Pi_u$ transition*, J. Chem. Phys. **94** (1991), 2401.

Schulte, J., Seifert, G. *DFT-LDA molecular-dynamics of molecular collision processes.* Chem. Phys. Lett. **221** (1994), 230.

Seifert, G., Schmidt, R. *Fusion and deep inelastic-scattering in c-60-c-60 collisions*, Int. J. Mod. Phys. B **6** (1992), 3845.

Seifert, G., Porezag, D., Frauenheim, T. *Calculations of molecules, clusters, and solids with a simplified LCAO-DFT-LDA scheme.* Int. J. Quant. Chem. **58** (1996), 185.

Slanina, Z., Kobayashi, K., Nagase, S. *Temperature development in a set of $C_{60}H_{36}$ isomers.* Chem. Phys. Lett. **382** (2003), 211.

Smith, D. *The ion chemistry of interstellar clouds*, Chem. Rev. **92** (1992), 1473.

Terentyev, A., Scholz, R., Schreiber, M., Seifert, G.: *Theoretical investigation of excited states of C_3*, J. Chem. Phys **121** (2004), 5767.

Tokaryk, D.W., Civiš, S., *Infrared emission spectra of C_3: the Renner effect in the $a^3\Pi_u$ and $b^3\Pi_g$ electronic states*, J. Chem. Phys. **103** (1995), 3928.